

Force Tolerances of Hybrid Nanodevices

Jacob J. Schmidt,[†] Xingqun Jiang,[‡] and Carlo D. Montemagno^{*,†}

Department of Bioengineering, UCLA, Los Angeles, California 91403, and
Cornell University, Ithaca, New York 14853

Received August 27, 2002; Revised Manuscript Received September 11, 2002

ABSTRACT

We have created hybrid devices consisting of nanoscale fabricated inorganic components integrated with and powered by a genetically engineered motor protein.¹ We wish to increase the assembly yield and lifetime of these devices through identification, measurement, and improvement of weak internal bonds. Using dynamic force spectroscopy, we have measured the bond rupture force of (histidine)₆ on a number of different surfaces as a function of loading rate. The bond sizes, lifetimes, and energy barrier heights were derived from these measurements. We compare the (His)₆–nickel bonds to other bonds composing the hybrid device and describe preliminary measurements of the force tolerances of the protein itself. Pathways for improvement of device longevity and robustness are discussed.

Introduction. Biomolecular motors have characteristics that conventional micro- and nanoelectromechanical systems (MEMS and NEMS) cannot match at present: moving parts nanometers in size, operation at speeds > 100 Hz for thousands of cycles without losing a single atom, and the ability to be produced routinely in micromole quantities in the laboratory. However, these motors pose constraints in material composition (protein only), they cannot be placed in arbitrary locations, and fueling and control are achieved through diffusion. Combining biomotors with micro- and nanofabricated systems may utilize the strengths of both.

Shown in Figure 1 is a depiction of a nanodevice made in our laboratory consisting of the biomolecular rotary motor F₁-ATPase mounted on a nickel-capped SiO₂ post with a nickel rod attached to the rotor.¹ The inorganic components of the device were fabricated using electron beam lithography and thermal evaporation. The protein was genetically engineered to contain a single cysteine on the γ and express histidine tags extending from the “bottom” of the β subunits. Histidine tags are commonly used in affinity purification with nickel nitrilotriacetic acid (Ni–NTA) and have been qualitatively shown to adhere to nickel metal as well.² The devices self-assembled through the sequential addition of the components: the motors, after biotin maleimide was attached to the cysteine on the rotor, were flowed into a chamber containing the fabricated glass slide, and the (His)₁₀ tags on the motor base attached to the nickel-capped posts. Following a rinse step, streptavidin was introduced to the chamber, bonding to the biotin. Separately, the nickel rods were functionalized with biotin after incubation with a short peptide sequence having (His)₆ on one end and cysteine–biotin on the other end. These functionalized rods were

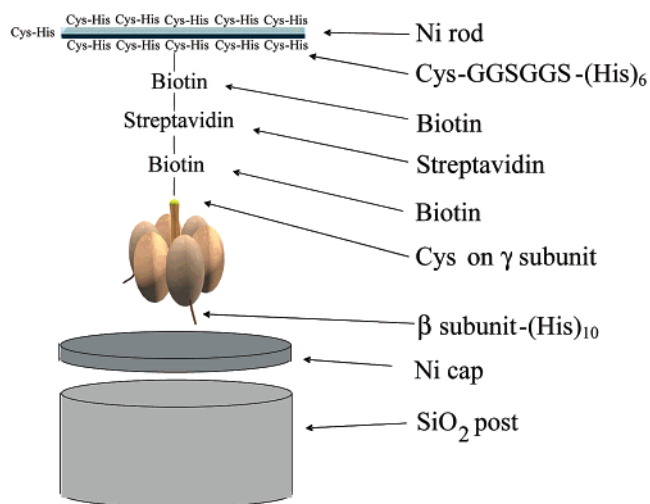


Figure 1. Exploded depiction and bonding scheme of the hybrid nanodevice powered by the biomolecular rotary motor F₁-ATPase. The device is sequentially self-assembled, resulting in a number of bonds in series. Each of these bonds has a characteristic lifetime, which decreases exponentially with force. The shortest bond lifetime effectively determines the lifetime of the device.

injected into the chamber and the device assembly was complete. Using light microscopy, the rods were observed to rotate at ~ 7 Hz following the addition of ATP.

Knowledge of the failure modes and rates is crucial in the engineering of any device. The multiple injection and rinse steps in the device assembly exert viscous drag forces; these forces are also present during operation of the device. The bonds holding the device together may not rupture immediately upon the introduction of these forces, but forces decrease bond lifetime exponentially.^{3,4} As the device yield was <0.01% and the maximum lifetime of the assembled devices was approximately 2 h, it is possible that these

* Corresponding author. E-mail: cdm@seas.ucla.edu

[†] UCLA.

[‡] Cornell University.

lifetimes were determined solely by a “weak link” in the bonding scheme shown in Figure 1. Knowledge of the binding strengths between different materials on the molecular level would allow strengthening of the weak links of this hybrid device and others and also enables rational device design.

In this paper, we show results of experimental studies of the bonds forming this device. The bonds in this device may be characterized in several distinct groups: covalent bonds, biospecific bonds, metal affinity (chelation), and the multiple aggregate van der Waals and hydrogen bonds which dictate secondary and tertiary protein structure. Within this very rough schema we can order the bonds of our device. Covalent bonds have been shown to be the strongest;⁵ therefore, in this work we have focused our attention on the biospecific bond of biotin–streptavidin and the metal affinity bond of (His)₆–nickel and also (His)₆–Ni–NTA and (His)₆–gold for comparison. We have used dynamic force spectroscopy to explore bond rupture force as a function of bond loading rate. Using Evans’ theory,⁴ we have used these measurements to calculate the characteristic bond length and lifetime as a function of force.

Experimental Section. The force spectroscopy experiments were performed using a Topometrix Explorer AFM, using Si₃N₄ cantilevers (Topometrix) with nominal spring constants of 32–64 pN/nm. The spring constant of each cantilever was measured using its thermal spectrum.⁶ The adhesion strengths between ligands on the tip and various surfaces were determined by bringing the tip into contact with the surface and retracting it at various speeds, measuring the force at which the bond to the surface ruptured. Hundreds of these rupture forces were measured for each loading rate and sample and plotted as histograms.

As a control, the biotin–streptavidin force was measured. The tip and a glass coverslip were incubated in 1 mg/mL biotinylated-bovine serum albumin (biotin-BSA) (Sigma) in PBS (20 mM phosphate, 150 mM NaCl, pH 7.5). The coverslip was then incubated with 1 mg/mL streptavidin (Sigma) in PBS for 2 h. All force spectroscopy experiments were performed in PBS. Incubation of the streptavidin–biotin-BSA surface with free biotin resulted in the loss of binding between the tip and the surface. The rupture force measurements were consistent with previously reported values⁷ and established a baseline for comparison with the (His)₆ adhesion measurements that followed.

In subsequent experiments the cantilevers were functionalized as follows: after washing with acetone, alcohol, and water, the cantilevers were further cleaned and freshly oxidized in a plasma cleaner (Harrick) for 1–3 min. The tips were then functionalized with (aminopropyl)triethoxysilane (Sigma) at 2% in acetone. A bifunctional cross-linker of *N*-hydroxysuccinimide-poly(ethylene glycol)-maleimide (MW 5400, Shearwater Polymer, Huntsville, AL) was attached to the silane by incubation with the cantilever at 3 mg/mL in acetone with 0.5% triethylamine for 1.5 h. Finally, the peptide CGGSGGSHHHHHH (Bio-Synthesis, Inc.) was attached to the linker at 1 mg/mL in PBS. To reduce nonspecific adhesion of the tip to the substrate, the tip was

incubated in 1 mg/mL BSA in PBS overnight. All measurements were performed in PBS.

A second control was performed in PBS at pH 7.5 using a glass slide incubated overnight with Ni–NTA conjugated with horseradish peroxidase (NTA-HRP) (Qiagen). Force measurements between this substrate and the (His)₆ tip yielded data consistent with published values.⁸ The effects of pH on this bond were explored by repeating this experiment at pH 6. Adhesion measurements between (His)₆ and glass slides coated with 15 nm of nickel and gold (electron beam evaporated over a 5 nm adhesion layer of chromium) were performed in PBS at pH 7.5. Bonding between the His tags and the surface was observed and measured for both.

Analysis. Each force data point was represented by Gaussians of unitary area with widths corresponding to the measurement uncertainty (10–20 pN). These Gaussians were then summed, and the resulting distribution was used to determine the peak force. The theory of Evans was used to analyze the peak rupture force data.⁴ For simple probe–ligand linkages, the peak force is related to the loading rate by the expression

$$f = \frac{k_B T}{x_\beta} \left[\ln(k_s v_t) + \ln\left(\frac{t_{\text{off}} x_\beta}{k_B T}\right) \right] \quad (1)$$

where $k_B T$ is thermal energy, x_β is the characteristic bond length, k_s is the spring constant of the probe, v_t is the tip velocity, and t_{off} is the bond lifetime at zero force. The product of k_s and v_t is the loading rate. If the ligand is attached to the probe through two flexible linkers in series, the spring constant in the above expression is force dependent and is replaced by

$$k_s(f) = \frac{\frac{1}{k_{\text{cant}}} + \frac{\partial x_1}{\partial f}(f) + \frac{\partial x_2}{\partial f}(f) + \frac{k_B T}{x_\beta} \left[\frac{\partial^2 x_1}{\partial f^2}(f) + \frac{\partial^2 x_2}{\partial f^2}(f) \right]}{\left(\frac{1}{k_{\text{cant}}} + \frac{\partial x_1}{\partial f}(f) + \frac{\partial x_2}{\partial f}(f) \right)^2} \quad (2)$$

where k_{cant} is the spring constant of the probe and $\partial x_1/\partial f(f)$ is the force-dependent compliance of the first flexible linker, and so on. We use Evans and Ritchie’s interpolation⁹ of a functional form for the extension-dependent force of the Freely Jointed Chain (FJC) model:

$$f(x) \approx \frac{k_B T}{b} \left[\frac{x \left[3 - \frac{2x}{L_p} \right]}{1 - \frac{x}{L_p}} \right] \quad (3)$$

where b is the persistence length and L_p is the fully stretched length of the polymer. Poly(glycine) has been shown to exhibit behavior consistent with the FJC model.¹⁰ The persistence length of PEG is 3.6 Å,¹¹ and that of the peptides is 3.8 Å.¹⁰ L_p of the MW 5400 PEG was calculated to be \approx

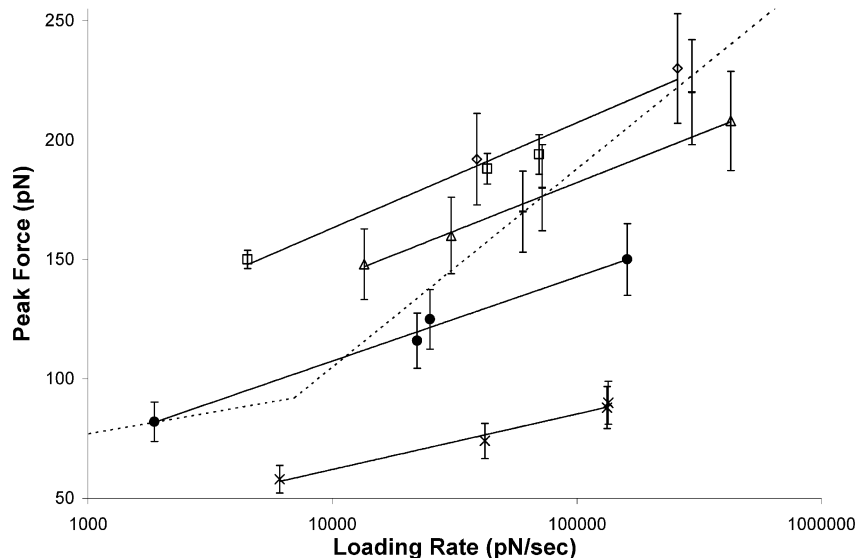


Figure 2. Plot of the peak rupture force versus loading rate for $(\text{His})_6$ with various substrates: Ni-NTA at pH 7.2 (\square), Ni-NTA at pH 7.5 (\diamond), Ni-NTA at pH 6.0 (\triangle), Ni at pH 7.5 (\bullet), and Au at pH 7.5 (\times). Also shown are measurements of biotin-streptavidin at pH 7.2 ($-$). Measurement uncertainties are due primarily to spring constant measurement, $\sim \pm 10\%$. The data of $(\text{His})_6$ on Ni-NTA at pH 7.2 are taken from ref 8, and the dashed line shows biotin-streptavidin data taken from ref 7.

Table 1: Measured Bonding Parameters between $(\text{His})_6$ and Four Substrates and Also Biotin-Streptavidin at Low (L) and High (H) Loading Rates

	Ni-NTA pH 7.2	Ni-NTA pH 6.0	Ni	Au	biotin- streptavidin
$x_\beta(\text{\AA})$	2.1	2.3	2.6	4.0	(L) 5.4, (H) 1.1
$t_{\text{off}}(\text{sec})$	9.6	5.6	1.7	.51	(L) 164, (H) 0.066
$\Delta\Delta E_b(k_B T)$	-2.8	-3.4	-4.6	-5.8	(L) 0, (H) -7.8

26 nm, and L_p of the peptides calculated as the length of CCGSGGS, ≈ 2.6 nm.

The peak force data are plotted versus loading rate in Figure 2. In the case of polymer linkers, the loading rates were self-consistently calculated from compliances at the rupture force using eqs 1–3. Previous data measuring the unbinding of $(\text{His})_6$ -Ni-NTA and biotin-streptavidin are shown for comparison and agree well. All data show a linear dependence on the logarithm of the loading rate, consistent with the theory at these forces, with the slope of the line related to the characteristic bond length and the intercept related to the bond length and zero force lifetime. This relationship breaks down when the forces are on the order of $k_B T/x_\beta$ and the probe stiffness is much greater than polymer stiffness.

The two free parameters of the above theory, x_β and t_{off} , were obtained from fits of the peak force data to eqs 1–3. These parameters are shown in Table 1. Many conclusions can be drawn from these data: the characteristic bond length of $(\text{His})_6$ -Ni-NTA at pH 6 is slightly larger than pH 7.2–7.5. However, the zero force lifetime, t_{off} , of the bond at pH 6 is significantly less, indicating a lower barrier height and a weaker bond. The poly(His)-Ni-NTA bond consists of two of the histidines coordinating around the Ni^{2+} ion held in place by four bonds to the NTA. The pK_a of histidine is 6.0–6.5,¹² implying that, on average, 50%–75% of the

imidazole rings of the $(\text{His})_6$ are protonated at a pH of 6, as opposed to $>90\%$ deprotonation at pH 7.5. This protonation prevents an unbonded lone pair of electrons on the double-bonded nitrogen of the imidazole ring from bonding to the Ni^{2+} . The NTA itself is unaffected by this pH range, with $\text{pK}_a \approx 2.2$.¹³ Unbinding and rebinding may be a possible mechanism responsible for the decreased lifetime at lower pH. If, following unbinding, the free histidines bound protons, the possibility of immediate rebinding to the NTA would be eliminated. If a sufficiently long time elapses before the His rebinds to the NTA, the ligand may diffuse away and is effectively permanently unbound. Obviously, is possible at all pH values, but is more likely and frequent at lower pH, explaining the shorter lifetime but similar bond lengths.

The data also show that $(\text{His})_6$ bonds to nickel, albeit more weakly. The bond length of $(\text{His})_6$ -nickel is greater than $(\text{His})_6$ -Ni-NTA, reflecting the change from sterically accessible and charged Ni^{2+} ions to a neutral planar metallic film. In comparison, the rupture force measurements and bond characteristics of $(\text{His})_6$ -gold are sufficiently different to show that these bonds are not explained merely by a nonspecific interaction with a solid surface or an element-independent His/metal bond.

The bond strengths may be ranked in a relative order based on the magnitudes of their lifetimes: the low loading rate regime of biotin-streptavidin is the strongest, followed by $(\text{His})_6$ -Ni-NTA at pH 7.5, $(\text{His})_6$ -Ni-NTA at pH 6, $(\text{His})_6$ -nickel, $(\text{His})_6$ -gold, and the high loading rate regime of biotin-streptavidin. For the bonds considered, at low forces the weak link is the $(\text{His})_6$ -nickel interface and at high forces the weak link is biotin-streptavidin. A Boltzmann activation above the energy barrier forming the bond results in a force-dependent lifetime of $t_{\text{lifetime}} = t_{\text{off}} e^{-f x_\beta / k_B T}$. At this point, the average lifetime of the device when subjected to various forces should be calculable.

However, the theory applied here and the experiments are valid only in a highly nonequilibrium regime where the force and velocity applied to the bond are sufficiently great that rebinding does not occur. At such large forces and loading rates, smaller outer energy barriers are immediately overwhelmed. At zero force, these barriers may prevent full unbinding or present a low barrier toward rebinding. Therefore, the zero force lifetimes derived from these measurements are not expected to be comparable to the lifetimes at equilibrium. This can readily be seen through the comparison of the 12 s lifetime measured for (His)₆-Ni-NTA to common affinity chromatography using the same system which can last many hours. Further, measurements in solution of biotin-streptavidin have indicated bound lifetimes greater than 50 hours.¹⁴ Previous experiments have also found 50 to 100,000-fold disparities between force spectroscopy and solution-based experiments.^{4,15} Further, our previous experiments with active devices allowed observation for several hours, an extremely improbable event if the zero-force lifetimes of Table 1 are correct.

Barrier heights may be compared using the following equation:⁴

$$\frac{\Delta\Delta E_b}{k_B T} \approx -\Delta\ln(\text{LoadingRate})_{f_{\text{peak}}=0} + \Delta\ln\left(\frac{k_B T}{x_\beta}\right) \quad (4)$$

where $\Delta\Delta E_b$ is the difference in barrier height of two bonds and is calculated using the difference in characteristic bond length and the difference in loading rate extrapolated at a peak rupture force of zero. The computed values are shown in Table 1. Taking the strongest bond, biotin-streptavidin at low force, as a baseline, we see that its barrier is $2.6 k_B T$ larger than that of (His)₆-Ni-NTA at pH 7.5, $4.6 k_B T$ larger than (His)₆-nickel, and so on. Rankings of bond strength based on energy barrier height are unchanged.

Conclusions. Complete knowledge of the force tolerances of our hybrid nanodevices is still incomplete, due to the lack of measurements on the protein itself. As the gamma subunit (the rotor) of the motor must be free to rotate, it is likely that it is the weakest component of the protein. We have initiated experiments with the protein; preliminary results may indicate that the protein is the weak link in the device (Figure 3). The work is ongoing. However, failure due to rotor pullout is susceptible only to forces emerging from and normal to the substrate. This situation is not the most common source of stress on the device, as in-plane forces caused by the laminar rinsing fluid flow (Reynolds number: $\sim 10^{-3}$) and rod rotation predominate. Components of these forces normal to the substrate are less than 0.1 pN. If the protein is not the weak link, the device lifetime is determined primarily by the lifetime of the (His)₆-nickel bond.

Previous work has indicated that F₁-ATPase rotates with a constant torque of ~ 40 pN nm.¹⁶ Assuming that the rod is attached at the middle and the force center halfway along the peptide chain, the reaction force on the (His)₆ is estimated to be 35 pN. A constant force has the effect of exponentially reducing bond lifetime; the 35 pN force on the (His)₆-nickel bond reduces the lifetime by a factor of 10. However, this

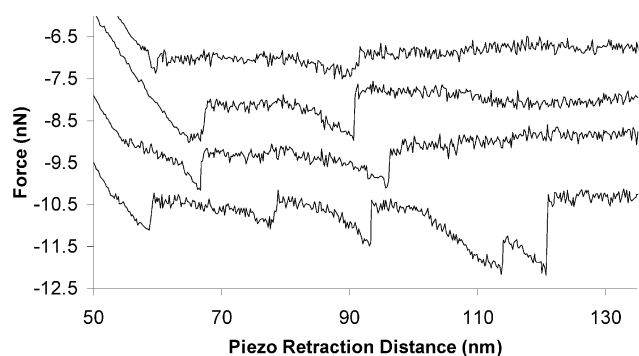


Figure 3. Four force-distance curves measuring rupture force of F₁-ATPase at a loading rate of 75 nN/sec (displaced horizontally and vertically for clarity). The proteins were attached to a gold-coated tip and gold-coated sample via the cysteine in the gamma subunit and additional cysteines added to the ends of the His tags on the motor base. Previous work has measured the sulfur-gold rupture force to be 1.4 ± 0.3 nN at a loading rate of 10 nN/sec⁵. Ruptures shown here could have resulted from the breakage of Au-S bonds, detachment of the protein nonspecifically adsorbed to the surface, pulling of the β subunits from the motor, pulling of the γ subunit out of the motor, or a force-induced denaturing of the protein. Rupture forces ranging from 20 pN to over 1 nN have been observed. Experiments are in progress.

is the lifetime of one bond. If other histidines are bonded to the nickel bonds, the protein may not detach from the rod and the unbound histidine has the opportunity to rebound. The reaction force on the peptides in the base is not significant when compared to those on the rotor, as the torque radius is over 10 times greater at the base (resulting in a force of 3 pN), and the base has three sets of peptides securing it.

The strength of the device could be improved through the substitution of a stronger bond for His₆-nickel. However, only a few peptide/inorganic substrate bonds are known. Recent work by Stanley Brown has found short peptide sequences that adhere specifically to iron oxide,¹⁷ gold, and chromium.¹⁸ Angela Belcher and co-workers, using phage-display techniques, have evolved peptides that adhere specifically and exclusively to GaAs(100), GaAs(111)A, GaAs(111)B, InP(100), and Si(100).¹⁹ As various biological organisms commonly bind to and direct the growth of many different materials, it is likely that an entire library of peptide sequences and inorganic substrates can be created. These peptide linkers do not necessarily need to be engineered into a larger protein; short heterobifunctional sequences can connect inorganic particles of heterogeneous composition.²⁰ Measurements of the binding strengths of these linkers would aid the design process and expand the range of materials and structures available, ultimately resulting in stronger devices with higher force tolerances and longer functional lifetimes.

Acknowledgment. This work was supported in part by NIST (grant number 60NANBOD0095).

References

- (1) Soong, R. K.; Bachand, G. D.; Neves, H. P.; Olkhovets, A. G.; Craighead, H. G.; Montemagno, C. D. *Science* **2000**, *290*, 1555-1558.

- (2) Soong, R. K.; Stelick, S. J.; Bachand, G. D.; Montemagno, C. D. In *Technical Proceedings of the Second International Conference on Modeling and Simulation of Microsystems*; San Juan, Puerto Rico, 1999.
- (3) Bell, G. I. *Science* **1978**, *200*, 618–627.
- (4) Evans, E. *Annu. Rev. Biophys. Biomol. Struct.* **2001**, *30*, 105–128.
- (5) Grandbois, M.; Beyer, M.; Rief, M.; Clausen-Schaumann, H.; Gaub, H. E. *Science* **1999**, *283*, 1727–1730.
- (6) Hutter, J. L.; Bechhoefer, J. *Rev. Sci. Instrum.* **1993**, *64*, 1868–1873.
- (7) Merkel, R.; Nassoy, P.; Leung, A.; Ritchie, K.; Evans, E. *Nature* **1999**, *397*, 50–53.
- (8) Kienberger, F.; Kada, G.; Gruber, H. J.; Pastushenko, V. P.; Riener, C.; Trieb, M.; Knaus, H.-G.; Schindler, H.; Hinterdorfer, P. *Single Mol.* **2000**, *1*, 59–65.
- (9) Evans, E.; Ritchie, K. *Biophys. J.* **1999**, *76*, 2439–2447.
- (10) Schimmel, P. R.; Flory, P. J. *PNAS* **1967**, *58*, 52–59.
- (11) Rex, S.; Zuckermann, M. J.; Lafleur, M.; Silvius, J. R. *Biophys. J.* **1998**, *75*, 2900–2914.
- (12) Stryer, L. *Biochemistry*, 4th ed.; W. H. Freeman and Company: New York, 1995.
- (13) Souaya, E. R.; Hanna, W. G.; Ismail, E. H.; Milad, N. E. *Molecules* **2000**, *5*, 1121–1129.
- (14) Chilkoti, A.; Stayton, P. *J. Am. Chem. Soc.* **1995**, *117*, 10622–10628.
- (15) Evans, E. *Faraday Discuss.* **1998**, *111*, 1–16.
- (16) Yasuda, R.; Noji, H.; Yoshida, M.; Kinosita, K.; Itoh, H. *Nature* **2001**, *410*, 898–904.
- (17) Brown, S. *PNAS* **1992**, *89*, 8651–8655.
- (18) Brown, S. *Nature Biotech.* **1997**, *15*, 269–272.
- (19) Whaley, S.; English, D.; Hu, E.; Barbara, P.; Belcher, A. *Nature* **2000**, *405*, 665–668.
- (20) Brown, S. *Nano Lett.* **2001**, *1*, 391–394.

NL025773V